The effect of isovalent doping on the electronic band structure of group IV semiconductors

Maciej P Polak[1,2] (ORCID)**, Paweł Scharoch**[2] **and Robert Kudrawiec**[2] (ORCID)

[1] Department of Materials Science and Engineering, University of Wisconsin-Madison, 1509 University Ave., Madison, WI 53706, United States of America
[2] Department of Semiconductor Materials Engineering, Faculty of Fundamental Problems of Technology, Wrocław University of Science and Technology, Wybrzeze Wyspiańskiego 27, Wrocław 50-370, Poland

E-mail: maciej.polak@pwr.edu.pl and robert.kudrawiec@pwr.edu.pl

Abstract

The band gap engineering of group IV semiconductors has not been well explored theoretically and experimentally, except for SiGe. Recently, GeSn has attracted much attention due to the possibility of obtaining a direct band gap in this alloy, thereby making it suitable for light emitters. Other group IV alloys may also potentially exhibit material properties useful for device applications, expanding the space for band gap engineering in group IV. In this work the electronic band structure of all group IV semiconductor alloys is investigated. Twelve possible A:B alloys, where A is a semiconducting host (A = C, Si, and Ge) and B is an isovalent dopant (B = C, Si, Ge, Sn, and Pb), were studied in the dilute regime (0.8%) of the isovalent dopant in the entire Brillouin zone (BZ), and the chemical trends in the evolution of their electronic band structure were carefully analyzed. Density functional theory with state-of-the-art methods such as meta-GGA functionals and a spectral weight approach to band unfolding from large supercells was used to obtain dopant-related changes in the band structure, in particular the direct band gap at the Γ point and indirect band gaps at the L(X) points of the BZ. Analysis of contributions from geometry distortion and electronic interaction was also performed. Moreover, the obtained results are discussed in the context of obtaining a direct fundamental gap in Ge:B (B = C, Sn, and Pb) alloys, and intermediate band formation in C:B (B = Sn and Pb) and Ge:C. An increase in localization effects is also observed: a strong hole localization for alloys diluted with a dopant of a larger covalent radius and a strong electron localization for alloys with a dopant of smaller radius. Finally, it is shown that alloying Si and Ge with other elements from group IV is a promising way to enhance the functionality of group IV semiconductors.

Supplementary material for this article is available online

Keywords: semiconductors, semiconductor alloys, highly mismatched alloys, band structure, group IV semiconductors

(Some figures may appear in colour only in the online journal)

1. Introduction

Group IV semiconductors (Si and Ge) are fundamental components of Si-based electronics, whereby semiconductor devices are grown on a Si substrate [1–4]. For low-dimensional heterostructures (e.g. quantum wells or quantum dots) which are the core of current devices, band gap engineering is necessary. It is most often achieved by alloying materials originating from the same group [5].

In IV group systems it is possible to mix Si with Ge in the full composition range and obtain an SiGe alloy with good structural, electrical and optical properties [1–5]. The parent materials are in the same crystal structure (diamond) and have similar lattice constants, electronegativities and ionization energies, factors important for the easy alloying of semiconductors. The SiGe alloy, however, has its own limitations. Throughout the entire composition range, it is an indirect band gap material which limits its application in optoelectronics. It also only covers the span of energy gaps between that of Si and Ge. Alloying Si and Ge with other compounds from group IV (C, Sn, and Pb) is more challenging and, therefore, less explored experimentally [5]. However, it opens the way for further band gap engineering of group IV semiconductors. It may not only provide the possibility to obtain a group IV alloy with a direct band gap, but also allow the covering of a wider range of band gaps and lattice parameters. Moreover, it is also interesting from a more fundamental point of view since C (diamond) is a wide gap material while Sn and Pb are metals.

Alloying Ge with Sn has been intensively explored experimentally in recent years because it allows for the creation of a material with a direct band gap and development of photonics integrated with the Si platform [6–12]. On the other hand, GeSn with around 25% Sn is a zero band gap semiconductor/semimetal [13], which is interesting from the viewpoint of new phenomena in solid state physics [14, 15]. Research suggests that alloying Ge with Sn in a broad composition range is possible with present technologies, i.e. molecular beam epitaxy or chemical vapor deposition [16–19]. In other cases, where the size mismatch between the host and dopant atoms is more significant (e.g. CSn or SiPb), alloying in the full composition range can be more challenging or even impossible. However, in all cases alloying in a low composition regime is most certainly possible by ion implantation and post implantation annealing [20, 21]. Despite this fact, in many cases this issue has still not be experimentally explored; i.e. the electronic band structure of most group IV alloys is still unknown. Therefore, the results of theoretical investigations such as the one presented here may motivate experimental researchers to pursue the synthesis and experimental characterization of group IV alloys.

From the point of view of Si-based technology, Si- and Ge-based alloys with low concentrations of C, Sn, and Pb are the most interesting since it is important to tune the conduction and valence bands without drastic modification of the lattice constant. Such conditions are typical for highly mismatched alloys (HMA), i.e. alloys composed of atoms with significant differences in valence radii, electronegativities and ionization energies [22–26].

Among group IV alloys, such conditions may be present in many systems, but the electronic band structure has not been extensively analyzed. Just a handful of published theoretical and experimental papers only for selected systems exist [27–39], and no cross-sectional work can be found for such alloys. This paper aims to provide a systematic study and comparison of the group IV alloys to offer valuable insight into chemical trends that have not been studied previously.
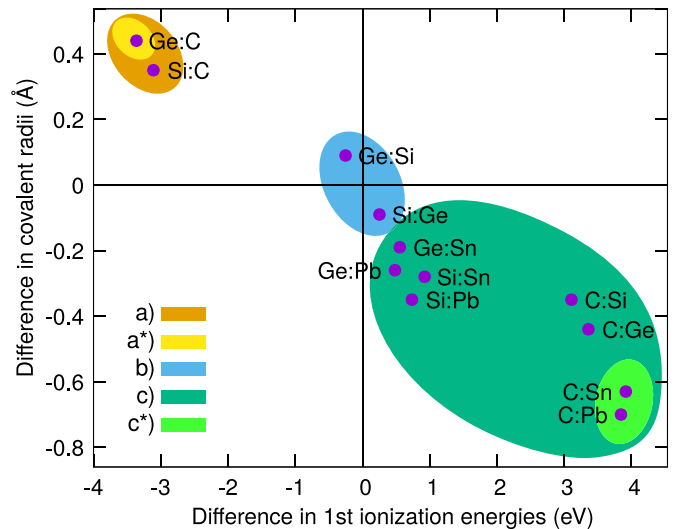
Figure 1. Differences in covalent radii [40] and first ionization energies [41] between the alloying elements as a representation of atomic mismatch. (a) HMAs where isovalent dopant is smaller and has higher ionization energy, (a*) subgroup of (a) where the magnitude of mismatch causes the emergence of an additional (conduction) band, (b) similar alloying elements (regular alloys), (c) HMAs where isovalent dopant is larger and has lower ionization energy, and (c*) subgroup of (c) where the magnitude of mismatch causes the emergence of an additional (valence) band.

In this work, we present systematic and comprehensive first principles density functional theory (DFT) studies of the effect of isovalent doping on the electronic band structure of group IV semiconductors. The obtained results are analyzed in terms of the influence of the optimization of the geometry (the distortion of atomic positions from pure material equilibrium) and the influence of element substitution on the changes in the electronic band structure. The observed changes in the electronic band structure are discussed in the context of the band anticrossing model, useful for simplified theoretical modeling of HMAs.

2. Results and discussion

To graphically show the mismatch between alloying elements, differences of covalent radii and first ionization energies between the alloying elements are presented in figure 1. Throughout the text the naming convention of A:B has been adopted, where A indicates the host material, while B stands for the isovalent dopant, i.e. a low composition alloy/solid solution. In figure 1, the studied alloys are grouped in terms of the mismatch: (a) HMAs where isovalent dopant is smaller and has higher ionization energy (significant changes in the conduction band), (a*) subgroup of (a) where the magnitude of mismatch causes the emergence of an additional (conduction) band, (b) similar alloying elements (regular alloys), (c) HMAs where isovalent dopant is larger and has lower ionization energy (significant changes in the valence band), and (c*) subgroup of (c) where the magnitude of mismatch causes the emergence of an additional (valence) band.

Table 1. Total change of the direct and indirect band gaps per 1% of the isovalent dopant. The columns are arranged in a similar fashion to figure 2 with rows representing the host material, and the columns representing the dopant. The indirect gap corresponds to the X valley in BZ for C and Si and the L point for Ge.

Direct (eV/1%)	C	Si	Ge	Sn	Pb
C	0	−0.134	−0.307	−1.022	−1.541
Si	0.019	0	−0.003	−0.024	−0.117
Ge	−0.593/0.140	0.024	0	−0.045	−0.099
Indirect (eV/1%)	C	Si	Ge	Sn	Pb
C	0	−0.158	−0.299	−0.961	−1.441
Si	−0.016	0	−0.002	−0.026	−0.075
Ge	−0.011	0.003	0	−0.030	−0.066

From the materials in the (a) and (c) groups, a different composition dependence of the band gap is expected than that in traditional semiconductor alloys (b), which will be discussed more in depth further in the text. The estimated band gap reductions (per 1% of the composition) were collected in table 1. The reduction of the gap is always higher than that expected from the virtual crystal approximation between host materials, indicating a stronger than linear change with composition. This can be described in various ways, depending on the type of alloying elements (equations (1)–(3), discussed later). Therefore, the parameters from table 1 should be considered as an approximation in the dilute regime (composition of up to a few percent). In all of the cases, except Si:C and Ge:Si, the band gap of the material is reduced due to alloying.
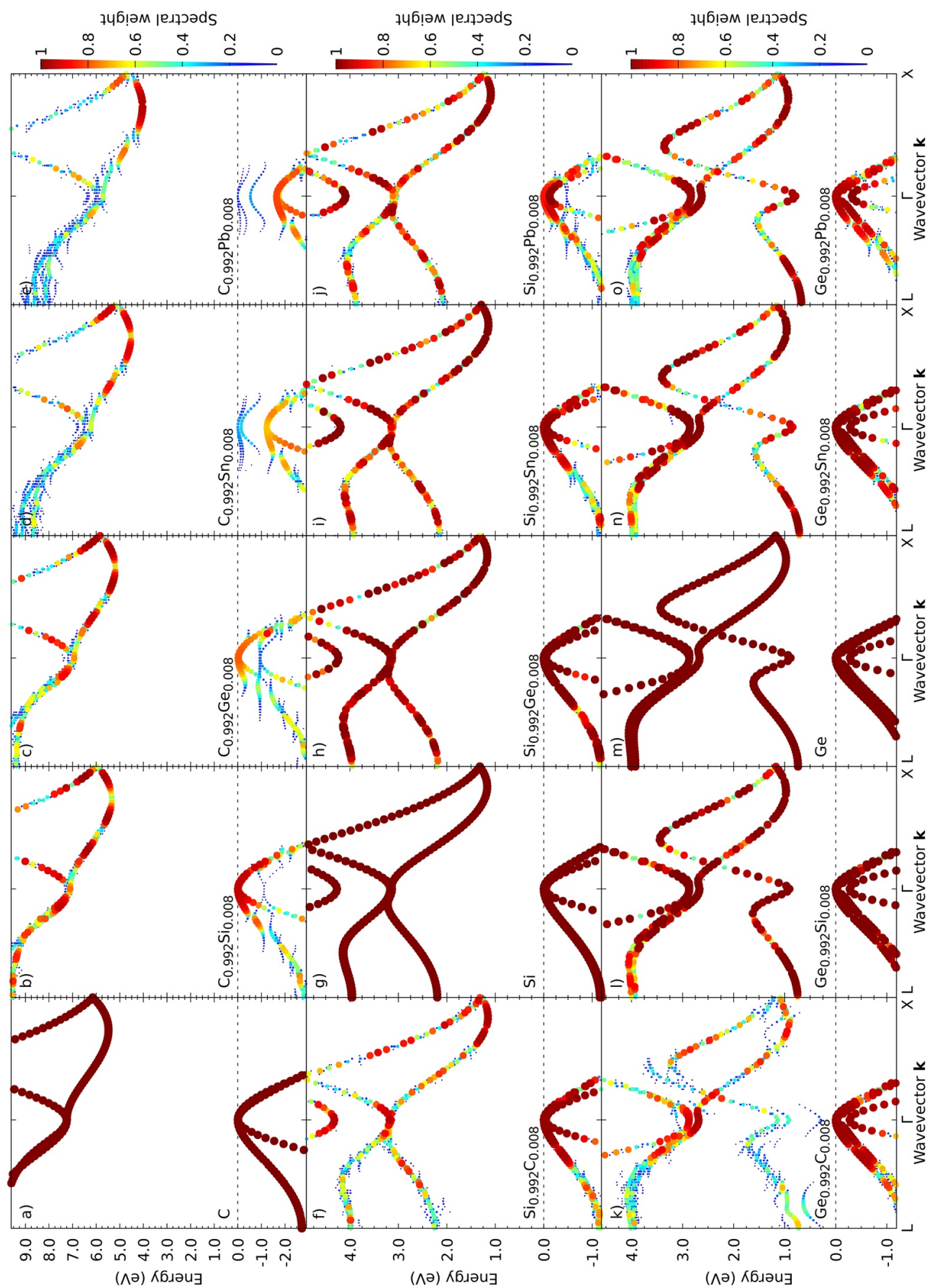
Figure 2 contains the unfolded band structures of all the studied alloys, C based, Si based and Ge based, respectively, with other group IV (C, Si, Ge, Sn and Pb) isovalent elements as dopants at $1/128 \approx 0.8\%$ composition. The logic of the rows and columns is arranged as follows: each row represents one host material, C, Si, and Ge, top to bottom, and each column represents one isovalent dopant, C, Si, Ge, Sn and Pb, left to right. Therefore, panels (a), (g), and (m) correspond to the pure host materials. For comparison, the material parameters for group IV materials involved here (including host materials and remaining dopants) are gathered in table 2.

The 0.8% concentration is obtained by replacing one of the atoms in a 128-atom supercell with an isovalent dopant. Using a single composition allows us to draw more meaningful conclusions about the chemical trends present within the entire family of the studied systems and direct comparison between them. The dilute regime is also most likely to be most relevant to real life applications, where the highly mismatched nature of the systems will only allow for the synthesis of low-concentration materials. The qualitative result of different band structures in figure 2 can be categorized into three groups: band structure almost unchanged (except for the change in the band gap) as in regular semiconductor alloys (Si:Ge and Ge:Si; figures 2(h) and (l)); significant changes in the Bloch character (spectral weights: color and size of the points) and disorder in the band structure mostly in the valence band (C:Si, C:Ge, C:Sn, S:Pb, Si:Sn, Si:Pb, Ge:Sn and Ge:Pb, figure 2 (b), (c), (d), (e), (i), (j), (n) and (o)); and similarly pronounced changes but mostly in the conduction band (Si:C and Ge:C, figures 2(f) and (k)). Among the latter two categories, in particular, the cases of C:Sn, C:Pb and Ge:C (figures 2(d), (e) and (k)) should be highlighted as those where distinct new bands appear. This categorization can be explained in terms of the mismatch between the host and isovalent dopant as seen in figure 1.

From table 1 it can be predicted that in some of the alloys, the possibility of a transition from an indirect to direct band gap exists. In order for this to happen, the reduction of the indirect gap has to be lower than that of the direct gap, and the band gap has to be wide enough to allow for the change in the band gap character while the gap is still present. The data in tables 1 and 2 allow for the estimation that, in line with previous studies, this certainly occurs for Ge:Sn, and it seems to be also possible for Ge:Pb. A particularly interesting behavior can be found for Ge:C, where a direct band gap is achieved by an additional band emerging inside the host Ge band gap due to the introduction of carbon (composed of carbon *s* orbitals). The other materials, although mostly exhibiting a higher reduction in the direct rather than indirect band gap, cannot accommodate such a transition for a composition low enough to keep the band gap open.

Apart from the very apparent conclusion about the chemical trends in the observed changes in the band structure, where the magnitude of the band gap reduction increases with the mismatch of the host and impurity atoms, the three specific cases of Ge:C, C:Sn and C:Pb are particularly interesting in terms of their unique band structure. The intermediate conduction band appearing in Ge:C, even for small concentrations of C, such as the 0.8% presented here, drastically changes the character of the material. Although both the host Ge and the impurity C are indirect band gap semiconductors, the influence of C atoms in the Ge host results in a direct gap material, suitable for light emission. In addition, the small admixture of C does not strongly influence the lattice constant of the Ge host, enabling growth Ge:C alloy on Ge or Si substrates. Because of this, Ge:C can be considered a good candidate for light emission within group IV semiconductor devices. Previously, a very similar change in the electronic band structure was observed for GaP diluted with nitrogen [42], where the indirect GaP host, after introducing even small amounts of nitrogen, exhibits photoluminescence [43, 44]. The similarity of the Ge:C suggests that even lower concentrations of C than the 0.8% studied here would allow this effect to take place.

Figure 2. Unfolded band structures of all the studied alloys organized row- and column-wise. The host material changes from top to bottom with increasing atomic number (C, Si, and Ge), while isovalent dopant changes from left to right with increasing atomic number (C, Si, Ge, Sn, and Pb).

Table 2. Material parameters obtained from calculations. See section 3 for more details.

	C	Si	Ge	Sn	Pb
a_0 (Å)	3.536	5.404	5.648	6.481	6.852
E_g^Γ (eV)	7.4	3.2	0.89	-0.39	-4.633
E_g^L (eV)	9.55	2.25	0.74	0.086	-1.99
E_g^X (eV)	5.57	1.21	0.97	0.711	0.028
c_{MBJ}	1.463*	1.114*	1.210*	1.197	1.212

The other two intriguing band structures of C:Sn and C:Pb do not seem to be promising for light emitters because of the indirect gap. Although clearly separate valence bands appear, which are promising in intermediate band solar cells [45], the very wide band gap of the host diamond strongly limits its application as a light absorber in solar cells. However, these alloys can be useful in other applications and they are themselves very interesting for better understanding solid state physics. For example, the presence of two valence sub-bands separated by a certain energy gap should result in a specific spectral dependence of absorption. The presence of the intermediate band in this case can help in the p-type doping of diamond.

Out of the 12 diluted alloys studied here, 2 (Si:Ge and Ge:Si, figure 1(a)) are well known as regular, well-matched semiconductor systems. The composition dependence of band gaps in these systems is well described by the quadratic Vegard's law:

$$E_g^{A_{1-x}B_x}(x) = (1-x)E_g^A + xE_g^B - bx(1-x), \quad (1)$$

where E_g^A and E_g^B are the band gaps of the host materials A and B, respectively, x is the composition, and b is a bowing parameter.

C:Si and Si:C are less similar to regular alloys since the spectral weights of wave functions significantly decrease for both the conduction and the valence band; see figure 2. In addition, the dopant-related change in the band gap is much larger than that observed for regular alloys, which in the case of group IV alloys are represented by SiGe; see table 1.

Very similar changes in the electronic band structure are observed for Ge:Sn. From our previous research [13] as well as from literature [23], it is known that Ge:Sn has different behavior than regular alloys, which can be attributed to the higher mismatch in size and electronegativity between Ge and Sn atoms, allowing this material to be classified as an HMA. A valence band anticrossing model (VBAC) has been shown to accurately reproduce the composition dependence of the band gap in this alloy [23] in the low-composition region. The composition-dependent band gap in the VBAC model is expressed by replacing the $bx(1-x)$ term in equation (1) with a two-parameter expression, dependent on the relative position of the impurity B atom resonant level to the valence band maximum (VBM), E_{BI}, and a parameter C_{BM} describing the magnitude of the interaction [46]. The equation then reads:

$$E_g^{A_{1-x}B_x}(x) = (1-x)E_g^A + xE_g^B - \frac{1}{2}\left(\sqrt{E_{BI}^2 + 4C_{BM}^2 x} - E_{BI}\right). \quad (2)$$

Since the magnitude of the interaction increases with the mismatch between the alloying elements [47–49], it is reasonable to expect similar behavior of seven other systems studied here, i.e. Ge:Pb, Si:Sn, Si:Pb, C:Si, C:Ge, C:Sn and C:Pb (figure 1(c)). From those, C:Sn and C:Pb are particularly interesting, as here due to the extreme mismatch (figure 1(c*)), a separate valence band emerges.

The remaining Ge:C alloy exhibits the opposite behavior, similar to the one observed in dilute nitrides such as GaP:N or GaAs:N [42], where the anticrossing takes place in the conduction band due to the opposite mismatch between the Ge and C atoms as compared to the mismatch between Ge and Sn/Pb. In this case, the conduction band is split into two unfilled sub-bands, E_- and E_+, according to the (conduction) band anticrossing model (BAC) [22]:

$$E_\pm^{A_{1-x}B_x}(x) = \frac{1}{2}\left(E_g^A + E_{BI} \pm \sqrt{\left(E_g^A - E_{BI}\right)^2 + 4C_{BM}^2 x}\right), \quad (3)$$

where, similarly to the VBAC case, E_{BI} is the energetic distance from the impurity atom resonant state to the VBM and C_{BM} is the magnitude of the interaction. It is worth noting that this equation, unlike equation (2), is only applicable in a regime of relatively low concentrations of impurities. This case is shown in figure 1(a*) and in figure 2(k).

The BAC parameters can be determined experimentally by studying the pressure dependence of the energies of the E_- and E_+ transitions [22] or the content dependence of these transitions [26]. In general, parameters for VBAC can be also obtained by experimental measurements of E_- and E_+ transitions, but the valence band is more complex than the conduction band, and to date, the E_- transition has not been clearly observed for any alloy described within the VBAC. For the same reason, the direct accurate extraction of the valence band anticrossing parameters is impossible from our calculations (i.e. three valence bands interacting with the impurity levels lead to a 6×6 Hamiltonian [23, 50] and, therefore, complex equations). However, a less rigorous ballpark estimate can be inferred for the BAC in the case of Ge:C. The two subbands observed in the band structures, corresponding to E_- and E_+ in equation (3), allow us to directly solve equation (3) for E_{BI} and C_{MB} at $x = \frac{1}{128}$. The solution yielded $E_{BI} \approx 0.43$ eV and $C_{MB} \approx 3.12$ eV.

In the case of VBAC, however, even though the values cannot be directly extracted, the analysis of the band structures in figure 2 allows us to draw a conclusion on the expected behavior of E_{BI} and C_{BM} parameters. The impurity level should
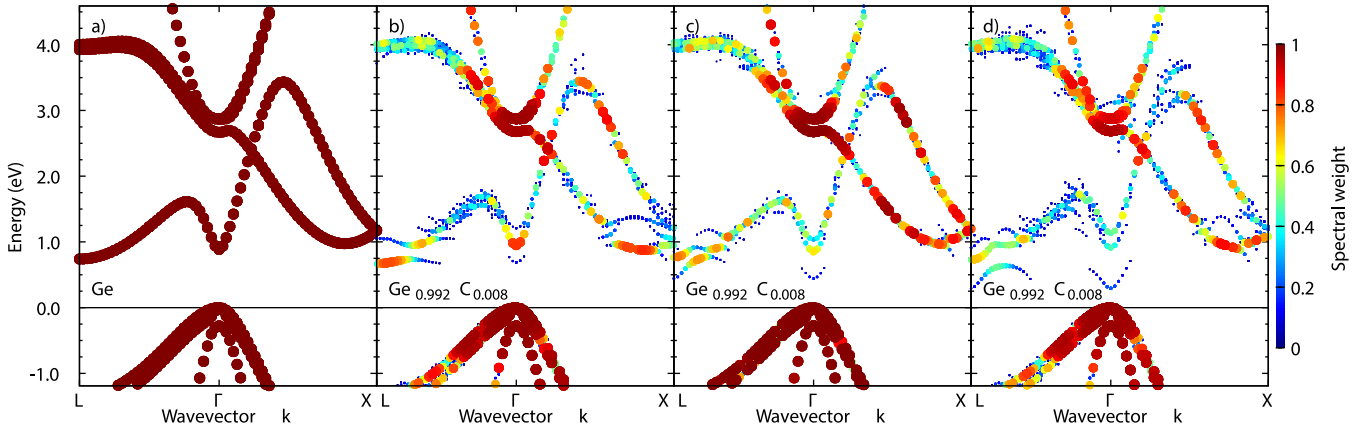
Figure 3. Unfolded band structures of Ge:C showing the contribution of geometry distortion (b) and electronic (c) to band gap change, together with the band structure of the Ge:C alloy (d) and pure Ge (a).

Table 3. Decomposition of direct band gap changes into geometric and electronic contributions. The indirect gap corresponds to the X valley in BZ for C and Si and the L point for Ge.

Material	Change of band gap in percent (eV) (geometry distortioncontribution)		Change of band gap in percent (eV) (electronic distortioncontribution)	
	direct	indirect	direct	indirect
C:Si	−0.082	−0.094	−0.029	−0.089
C:Ge	−0.122	−0.161	−0.143	−0.153
C:Sn	−0.272	−0.439	−0.924	−0.826
C:Pb	−0.394	−0.691	−1.724	−1.552
Si:C	0.016	−0.051	0.006	0.003
Si:Ge	0.001	0.004	−0.003	−0.003
Si:Sn	0.002	0.000	−0.018	−0.016
Si:Pb	0.002	−0.005	0.008	−0.033
Ge:C	0.061	−0.073	0.059	0.026
Ge:Si	0.006	0.000	0.014	0.003
Ge:Sn	−0.037	−0.016	0.009	−0.014
Ge:Pb	−0.057	−0.029	−0.022	−0.024

be closer to the valence band edge as the radius of the isovalent dopant increases and ionization energy decreases. Similarly, the interaction energy should increase. This is most easily noticeable in figures 2(b)–(e). The visual analysis of the unfolded band structures in figure 2 allows for another qualitative conclusion. The Bloch spectral weight is connected to the localization of states, which increases with the decrease in spectral weight [51]. Here, again, the loss of spectral weights follows the trends of mismatch (figure 1), with the most disorder and highest loss of Bloch character for the most mismatched alloys.

To gain better insight into the origin of the observed changes in the electronic band structure, additional calculations were performed, where the analysis of alloys was separated into two contributions: the influence of the distortion in geometry (the ion coordinates) and the influence of the elements' substitution. The first one was obtained by using the crystal structure optimized for the alloy, but keeping the material pure by populating the atomic sites with only the host material atoms. Second, the crystal structure has been kept undisturbed in the equilibrium diamond structure ionic positions, but the atoms have been replaced to form an alloy. This

approach allowed us to decompose the geometric and atomic contributions to the changes of the electronic band structure and its features. The results in terms of the change in band gap per 1% of the isovalent dopant are gathered in table.

Figure 3 presents an example of the unfolded band structures for the three cases: 1. only the optimized lattice geometry distortion included (figure 3(b)); 2. only the electronic effects included (element substitution, figure 3(c)); 3. all effects taken into account (geometry optimization and element substitution, figure 3(d)); as well as a pure material for comparison (figure 3(a)). The band gap reduction decomposition for the remaining 11 materials presented in a similar fashion to this in figure 3 is gathered in the supplementary material in figures S1–S11 (https://stacks.iop.org/JPD/54/085102/mmedia). From the analysis of this data, it is clearly visible that the change of the band structure can be attributed to both the lattice geometry distortion and the electronic contribution of the introduced atom. Often the magnitude of the two contributions is comparable. Table 3 shows that as the mismatch between the atoms increases, the contribution of the local lattice distortion plays an increasingly important role in the band structure change. This indicates that virtual crystal-like approximations

such as the alchemical mixing method [52], unable to account for the changes in geometry, should be avoided. This is in addition to the already mentioned strongly non-linear overall band gap reduction.

The presented studies of the electronic band structure of the diluted group IV semiconductors have been discussed in the context of their potential applications in light emitters or solar cells. However, the most interesting study seems to be the discussion of changes in the electronic band structure in the context of chemical trends. For the studied alloys, the electronic band structure changes mainly in the valence band when small atoms are replaced by large atoms; see all C:B alloys, where B is the isovalent dopant, Si:Sn and Si:Pb. The opposite behavior is observed when large atoms are replaced by small atoms; see Ge:C, which is the opposite situation to C:Ge. For all these alloys, the spectral weight of wavefunction strongly decreases for the modified band. It means a strong hole (electron) localization for IV alloy diluted with a dopant of a larger (smaller) valence radius. For remaining alloys, changes in the electronic band structure are comparable for both the conduction and the valence band. For Si:Ge and Ge:Si, these changes are very small since differences in electronegativities, ionization energies and atomic radii are very small for Si and Ge.

In general similar chemical trends can be expected for group III–V and II–VI semiconductors, but these material systems are more difficult to investigate and interpret because of the anion and cation sublattice. The group IV family of alloys is the simplest system, which varies from semiconductors with a wide gap (diamond) to metals (lead), and is therefore interesting to consider, even if some of these alloys may be difficult to synthesize.

3. Methods

The alloys were modeled using a 128-atom supercell ($4 \times 4 \times 4$ multiplication of a primitive two-atom unit cell). In each supercell, one host atom was replaced with the alloying element in order to obtain a dilute concentration of around 0.8%. The LDA exchange-correlation functional [53] was used in the geometry optimization since for the studied group-IV materials it has been proven to outperform the other functionals [54]. For the alloys, the internal atom positions were fully optimized for a fixed lattice constant given as a linear interpolation between the pure hosts' material in their diamond crystal structure.

The electronic band structure was calculated with the mBJLDA functional [55] to overcome the problem of band gap underestimation in LDA. Even though the mBJLDA functional reproduces the band gap of group IV semiconductors with relatively high accuracy [55, 56], the *c* parameter for host materials was slightly increased (by no more than 5% from the self-consistently calculated value; see table 2) to achieve perfect agreement with the 0 K values well established in experimental measurements [5]. For Sn and Pb, since their band structure in the diamond crystal lattice is not experimentally known, it has been calculated self consistently. The *c* parameter used to calculate the electronic band structure has been

obtained as a linear interpolation of the values for the parent materials. This approach has been thoroughly tested and proven to be very successful in our previous work [13] as well as in other research [57].

The lattice constants obtained for the pure host materials, as well as the self-consistent and adjusted values of the *c* parameters, together with the obtained band gap values are presented in table 2. The supercell approach produces a band structure obfuscated by the band folding due to the reduction of the Brillouin zone (BZ). To recover the full primitive BZ band dispersion, the spectral weight approach to band unfolding was used [58, 59], by the means of the `fold2bloch` code [60].

Convergence studies of the control parameters were performed and as a result, a $2 \times 2 \times 2$ Monkhorst–Pack k-point mesh [61] (an equivalent of an $8 \times 8 \times 8$ mesh in the primitive unit cell) was used, with 10^{-3} eV Å^{-1} tolerance on the maximum residual force in the geometry optimization and 10^{-6} eV total energy convergence in the electronic band structure calculations.

Spin–orbit interactions were included in all calculations. The recommended set of PAW potentials [62] was used, with the *s* and *p* states treated as valence in C, Si and Ge, and additionally taking into account *d* states in the heavier Sn and Pb. All DFT calculations were performed using the VASP package [63, 64].

4. Summary

The effect of isovalent doping on the electronic band structure of group IV semiconductors has been studied within the DFT with state-of-the-art methods including the meta-GGA mBJLDA functional and band unfolding based on the spectral weight approach. It has been found that the dopant-related changes in the band gap (both direct and indirect) occur according to chemical trends in differences (mismatch) in atom radii and ionization energies. The changes in band structure are accompanied by an increase in localization of electronic states, indicated by a loss of Bloch character of conduction and valence bands. Moreover, it has been concluded that a direct gap can be achieved in Ge via alloying with C, Sn or Pb. In the case of Ge:C the direct band gap is achieved by the emergence of an intermediate empty band below the conduction band minimum. In the two other cases, Ge:Sn and Ge:Pb, the direct band gap is achieved due to a faster rate of reduction of the direct band gap than the indirect band gap as a function of composition. The same effects are most likely impossible to achieve in C and Si by alloying with low compositions of other group IV elements since the electronic band structure of the host material is strongly indirect; i.e. the energy difference between the direct and indirect gap is much larger than the dopant-related changes in band gaps. The tuning of the band gap from indirect to direct in Ge strongly enhances the functionality of group IV semiconductors since it can make them more useful for optoelectronics, i.e. the field that until now has been dominated by III–V semiconductors. The influence of local lattice optimization has been investigated as well, revealing that it has a significant effect on the modification

J. Phys. D: Appl. Phys. **54** (2021) 085102

M P Polak *et al*

of the band structure, in particular in alloys with a high mismatch, and should not be dismissed. Another important finding is the formation of an intermediate band, which has been clearly observed in the conduction band for Ge diluted with C and in the valence band for C diluted with Sn and Pb. This property can also expand the functionality of group IV semiconductors, since materials with intermediate bands may have perspectives for use in a new generation of solar cells or other applications.

Acknowledgments

ORCID iDs

Maciej P Polak ⬤ https://orcid.org/0000-0001-7198-7779
Robert Kudrawiec ⬤ https://orcid.org/0000-0003-2593-9172

References

[1] Paul D J 2004 Si/SiGe heterostructures: from material and physics to devices and circuits *Semicond. Sci. Technol.* **19** R75

[2] Shiraki Y and Sakai A 2005 Fabrication technology of SiGe hetero-structures and their properties *Surf. Sci. Rep.* **59** 153

[3] Lee E A, Fitzgerald M L, Bulsara M T, Currie M T and Lochtefeld A 2005 Strained Si, SiGe and Ge channels for high-mobility metal-oxide-semiconductor field-effect transistors *J. Appl. Phys.* **97** 011101

[4] Aqua J-N, Berbezier I, Favre L, Frisch T and Ronda A 2013 Growth and self-organization of SiGe nanostructures *Phys. Rep.* **522** 59

[5] Adachi S 2009 *Properties of Semiconductor Alloys: Group-IV, III-V and II-VI Semiconductors* (Hoboken, NJ: Wiley)

[6] Wirths S *et al* 2015 Lasing in direct-bandgap GeSn alloy grown on Si *Nat. Photon.* **9** 88

[7] Al-Kabi S *et al* 2016 An optically pumped 2.5 μm GeSn laser on Si operating at 110 K *Appl. Phys. Lett.* **109** 171105

[8] Stange D *et al* 2016 Optically Pumped GeSn Microdisk Lasers on Si *ACS Photonics* **3** 1279

[9] Reboud V *et al* 2017 Optically pumped GeSn micro-disks with 16% Sn lasing at 3.1 μm up to 180 K *Appl. Phys. Lett.* **111** 092101

[10] Margetis J *et al* 2018 Si-Based GeSn Lasers with Wavelength Coverage of 2-3 μm and Operating Temperatures up to 180 K *ACS Photonics* **5** 827

[11] Dou W *et al* 2018 Optically pumped lasing at 3 μm from compositionally graded GeSn with tin up to 22.3. *Opt. Lett.* **43** 4558

[12] Thai Q M *et al* 2018 GeSn heterostructure micro-disk laser operating at 230 K *Opt. Express* **26** 32500

[13] Polak M P, Scharoch P and Kudrawiec R 2017 The electronic band structure of Ge$_{1-x}$Sn$_x$ in the full composition range: indirect, direct and inverted gaps regimes, band offsets and the Burstein-Moss effect, *J. Phys. D: Appl. Phys.* **50** 195103

[14] Manna K, Sun Y, Muechler L, Kübler J and Felser C 2018 Heusler, Weyl and Berry *Nat. Rev. Mater.* **3** 244–56

[15] Ozawa T *et al* 2019 Topological photonics *Rev. Mod. Phys.* **91** 015006

[16] Oehme M, Kostecki K, Schmid M, Oliveira F, Kasper E and Schulze J 2014 Epitaxial growth of strained and unstrained GeSn alloys up to 25% Sn *Thin Solid Films* **557** 169

[17] Wirths S, Buca D and Mantl S 2016 Si-Ge-Sn alloys: From growth to applications *Prog. Cryst. Growth Charact. Mater.* **62** 1

[18] Xu C, Wallace P M, Ringwala D A, Chang S L Y, Poweleit C D, Kouvetakis J and Menéndez J 2019 Mid-infrared (3–8 μm) Ge1-ySny alloys (0.15 < y < 0.30): Synthesis, structural and optical properties *Appl. Phys. Lett.* **114** 212104

[19] Azrak E, Chen W, Moldovan S, Duguay S, Pareige P and Cabarrocas P R I 2019 Low-Temperature Plasma-Assisted Growth of Core–Shell GeSn Nanowires with 30% Sn, *J. Phys. Chem* **124** 1220

[20] Prucnal S *et al* 2018 Strain and Band-Gap Engineering in Ge-Sn Alloys via P Doping *Phys. Rev. App.* **10** 064055

[21] Prucnal S *et al* 2019 Band gap renormalization in n-type GeSn alloys made by ion implantation and flash lamp annealing *J. Appl. Phys.* **125** 203105

[22] Shan W, Walukiewicz W, Ager J W, Haller E E, Geisz J F, Friedman D J, Olson J M and Kurtz S R 1999 Band anticrossing in GaInNAs Alloys *Phys. Rev. Lett.* **82** 1221

[23] Alberi K, Blacksberg J, Bell L D, Nikzad S, Yu K M, Dubon O D and Walukiewicz W 2008 Band anticrossing in highly mismatched Sn$_x$Ge$_{1-x}$ semiconducting alloys *Phys. Rev.* B **77** 073202

[24] Welna M, Kudrawiec R, Nabetan Y and Walukiewicz W 2014 Band anticrossing in ZnOSe highly mismatched alloy *App. Phys. Express* **7** 071202

[25] Kudrawiec R, Luce A V, Gladysiewicz M, Ting M, Kuang Y J, Tu C W, Dubon O D, Yu K M and Walukiewicz W 2014 Electronic band structure of GaN$_x$P$_y$As$_{1-x-y}$ highly mismatched alloys: suitability for intermediate-band solar cells *Phys. Rev. App.* **1** 034007

[26] Kudrawiec R and Walukiewicz W 2019 Electromodulation spectroscopy of highly mismatched alloys *J. Appl. Phys.* **126** 14110

[27] Yang J, Hu H, Miao Y, Wang B, Wang W, Su H and Ma Y 2020 Single-crystalline GePb alloys formed by rapid thermal annealing-induced epitaxy *J. Phys. D: Appl. Phys.* **53** 265105

[28] Liu X, Zheng J, Li X, Liu Z, Zuo Y, Xue C and Cheng B 2019 Study of GePb photodetectors for shortwave infrared detection *Opt. Express* **27** 18038

[29] Stephenson C A *et al* 2016 Band structure of germanium carbides for direct bandgap silicon photonics *J. Appl. Phys.* **120** 053102

[30] Liu X, Zheng J, Zhou L, Liu Z, Zuo Y, Xue C and Cheng B 2019 Growth of single crystalline GePb film on Ge substrate by magnetron sputtering epitaxy *J. Alloys Compd.* **785** 228

[31] Huang W, Cheng B, Xue C and Yang H 2017 The band structure and optical gain of a new IV-group alloy GePb: A first-principles calculation *J. Alloys Compd.* **701** 816

[32] Hussain A M, Singh N, Fahad H, Rader K, Schwingenschlögl U and Hussain M 2014 Exploring SiSn as a performance enhancing semiconductor: A theoretical and experimental approach *J. Appl. Phys.* **116** 224506

[33] Levard H, Laribi S and Guillemoles J-F 2014 Phonon lifetime in SiSn and its suitability for hot-carrier solar cells *Appl. Phys. Lett.* **104** 222106

[34] Huang W, Cheng B, Xue C and Li C 2014 Comparative studies of clustering effect, electronic and optical properties for GePb and GeSn alloys with low Pb and Sn concentration *Physica B: Condensed Matter* **443** 43

J. Phys. D: Appl. Phys. **54** (2021) 085102

M P Polak *et al*

[35] Zhang X, Ying C, Li Z and Shi G 2012 First-principles calculations of structural stability, elastic, dynamical and thermodynamic properties of SiGe, SiSn, GeSn *Superlattices Microstruct.* **52** 459

[36] Liu Q-J, Liu Z-T, Che X-S, Feng L-P and Tian H 2011 First-principles calculations of the structural, elastic, electronic, chemical bonding and optical properties of zinc-blende and rocksalt GeC *Solid State Sci.* **13** 2177

[37] Okinaka M, Miyatake K, Ohta J and Nunoshita M 2003 Large band gap bowing of MBE-grown GeC/Si(001) layers *J. Cryst. Growth* **255** 273

[38] Gulyas I A, Stephenson C A, Meng Q, Bank S R and Wistey M A 2019 The carbon state in dilute germanium carbides arXiv:1910.07258

[39] Broderick C A, Dunne M D, Tanner D S P and O'Reilly E P 2019 Electronic structure evolution in dilute carbide $Ge_{1-x}C_x$ alloys and implications for device applications *J. Appl. Phys.* **126** 195702

[40] Cordero B, Gómez V, Platero-Prats A E, Revés M, Echeverría J, Cremades E, Barragán F and Alvarez S 2008 Covalent radii revisited *Dalton Trans.* **2008** 2832–8

[41] Lide D 2003 *CRC Handbook of Chemistry and Physics : a Ready-Reference Book of Chemical and Physical Data* (Boca Raton, FL: CRC Press)

[42] Polak M P, Kudrawiec R and Rubel O 2019 Electronic band structure of nitrogen diluted Ga(PAsN): Formation of the intermediate band, direct and indirect optical transitions and localization of states, *J. Appl. Phys.* **126** 175701

[43] Xin H P, Tu C W, Zhang Y and Mascarenhas A 2000 Effects of nitrogen on the band structure of GaN_xP_{1-x} alloys *Appl. Phys. Lett.* **76** 1267

[44] Buyanova I A, Rudko G Y, Chen W M, Xin H P and Tu C W 2002 Radiative recombination mechanism in GaN_xP_{1-x} alloys *Appl. Phys. Lett.* **80** 1740

[45] Luque A and Martí A 1997 Increasing the Efficiency of Ideal Solar Cells by Photon Induced Transitions at Intermediate Levels *Phys. Rev. Lett.* **78** 5014

[46] Kudrawiec R, Kopaczek J, Polak M P, Scharoch P, Gladysiewicz M, Misiewicz J, Richards R D, Bastiman F and David J P R 2014 Experimental and theoretical studies of band gap alignment in $GaAs_{1-x}Bi_x$/GaAs quantum wells *J. Appl. Phys.* **116** 233508

[47] Vurgaftman I and Meyer J R 2003 Band parameters for nitrogen-containing semiconductors *J. Appl. Phys.* **94** 3675

[48] Wełlna M, Kudrawiec R, Nabetani Y, Tanaka T, Jaquez M, Dubon O D, Yu K M and Walukiewicz W 2015 Effects of a semiconductor matrix on the band anticrossing in dilute group II-VI oxides *Semicond. Sci. Technol.* **30** 085018

[49] Polak M P, Scharoch P and Kudrawiec R 2015 First-principles calculations of bismuth induced changes in the band structure of dilute Ga-V-Bi and In-V-Bi alloys: chemical trends versus experimental data *Semicond. Sci. Technol.* **30** 094001

[50] Alberi K *et al* 2007 Valence-band anticrossing in mismatched III-V semiconductor alloys *Phys. Rev.* B **75** 045203

[51] Pashartis C and Rubel O 2017 Localization of Electronic States in III-V Semiconductor Alloys: A Comparative Study *Phys. Rev. App.* **7** 064011

[52] Scharoch P, Winiarski M and Polak M 2014 Ab initio study of $In_xGa_{1-x}N$ - Performance of the alchemical mixing approximation *Comput. Mater. Sci.* **81** 358

[53] Perdew J and Wang Y 1992 Accurate and simple analytic representation of the electron-gas correlation energy *Phys. Rev.* B **45** 13244

[54] Haas P, Tran F and Blaha P 2009 Calculation of the lattice constant of solids with semilocal functionals *Phys. Rev.* B **79** 085104

[55] Tran F and Blaha P 2009 Accurate band gaps of semiconductors and insulators with a semilocal exchange-correlation potential *Phys. Rev. Lett.* **102** 226401

[56] Koller D, Tran F and Blaha P 2011 Merits and limits of the modified Becke-Johnson exchange potential *Phys. Rev.* B **83** 195134

[57] Landmann M *et al* 2013 Transition energies and direct-indirect band gap crossing in zinc-blende $Al_xGa_{1-x}N$, *Phys. Rev.* B **87** 195210

[58] Popescu V and Zunger A 2010 Effective band structure of random alloys *Phys. Rev. Lett.* **104** 236403

[59] Popescu V and Zunger A 2012 Extracting E versus k - Effective band structure from supercell calculations on alloys and impurities *Phys. Rev.* B **85** 085201

[60] Rubel O, Bokhanchuk A, Ahmed S and Assmann E 2014 Unfolding the band structure of disordered solids: From bound states to high-mobility Kane fermions *Phys. Rev.* B **90** 115202

[61] Monkhorst H J and Pack J D 1976 Special points for Brillouin-zone integrations *Phys. Rev.* B **13** 5188

[62] Kresse G and Joubert D 1999 From ultrasoft pseudopotentials to the projector augmented-wave method *Phys. Rev.* B **59** 1758

[63] Kresse G and Furthmüller J 1996 Efficiency of ab-initio total energy calculations for metals and semiconductors using a plane-wave basis set *Comput. Mater. Sci.* **6** 15

[64] Kresse G and Furthmüller J 1996 Efficient iterative schemes for ab initio total-energy calculations using a plane-wave basis set *Phys. Rev.* B **54** 11169